PBAF's genomic binding dynamics are regulated via bromodomain-acetyl-lysine interactions and select chromatin states.

Charles A. Kenworthy[1], Vincent Wong[1], Patrycja Dziuba[1], Luke D. Lavis[2], Wei-Li Liu[1], Robert H. Singer[1], and Robert A. Coleman[1*]

Author Affiliations:

1. Department of Anatomy and Structural Biology, Albert Einstein College of Medicine, Bronx, New York 10461, USA
2. Janelia Research Campus, Howard Hughes Medical Institute, Ashburn, Virginia, 20147

***To whom correspondence should be addressed:**
Gruss-Lipper Biophotonics Center, Department of Anatomy and Structural Biology, Albert Einstein College of Medicine, Bronx, NY 10461 Tel: 718-430-8623; Email: robert.coleman2@einstein.yu.edu

Shortened Title: PBAF chromatin binding dynamics

Keywords: PBAF, chromatin remodeling, Histone acetylation, Histone H3.3, Single Particle Tracking, bromodomain.

Abstract

Rapid changes in chromatin structure via the action of ATP-dependent chromatin-remodeling complexes are thought to dynamically regulate transcriptional bursting. Chromatin-remodeling complexes are targeted to genomic loci by histone post-translational modifications (PTMs) including acetylation. Despite extensive in vitro studies, much is still unknown about how chromatin-remodeling complexes rapidly bind genomic targets and function in vivo. We sought to understand how the PBAF chromatin-remodeling complex interacts with different chromatin states using live-cell single particle tracking of the BAF180 subunit. Dual color tracking of PBAF with either H3.3 or HP1α, revealed that PBAF binds chromatin within actively transcribed regions for shorter time periods relative to heterochromatin. We also found that deletion of BAF180's six bromodomains reduced both the association and dissociation of PBAF with chromatin. Finally, elevation of histone acetylation levels increased the frequency of PBAF revisiting to genomic foci. Together, these results suggest that acetyl-lysine dependent clustered binding of PBAF to select genomic loci may facilitate rapid chromatin-remodeling in actively transcribed regions. Overall our work also indicates that the dynamics of chromatin state alterations proceed at fast timescales to potentially regulate transcriptional bursting.

Introduction

Transcription of many genes occurs in a series of stochastic bursts interspersed with periods of inactivity (Larson et al. 2011; Sanchez and Golding 2013; Senecal et al. 2014). It is generally thought that changes in chromatin structure plays a major role in regulating the dynamics of transcriptional bursting (Metivier et al. 2003; Raser and O'Shea 2004; Tirosh and Barkai 2008; Tirosh et al. 2009; Sanchez et al. 2013). At enhancers and promoters of actively transcribing genes, chromatin disruption is likely facilitated by dynamic histone post-translational modifications that aid destabilization of histone-DNA interactions (Hebbes and Allen 2000; Sun et al. 2007; Calo and Wysocka 2013). In addition, dynamic incorporation of histone variants, such as H3.3 and H2A.Z further destabilizes nucleosomes to potentially regulate transcriptional bursting (Jin and Felsenfeld 2007; Henikoff et al. 2009; Jin et al. 2009; Calo and Wysocka 2013). Finally, the repeated action of ATP-dependent chromatin remodelers also plays a key role in destabilizing arrays of nucleosomes in transcriptionally active regions (Parnell et al. 2008; Lorch et al. 2011; Marathe et al. 2017).

After chromatin is remodeled, the promoter becomes permissive to transcription. RNA Polymerase II (Pol II) is then rapidly loaded onto the promoter every 4-8 seconds forming convoys of Pol II lasting for minutes (Tantale et al. 2016). The rapid kinetics of transcription initiation presumably necessitates chromatin remodeling on fast time-scales of seconds. Despite years of detailed in vitro studies, it is still unclear how chromatin-remodeling enzymes dynamically target and regulate changes to chromatin structure in vivo.

In addition to helping destabilize nucleosomes, histone acetylation aids localization of chromatin-remodelers and subsequent nucleosome removal from transcriptionally active regions (Jenuwein and Allis 2001; Boeger et al. 2003; Boeger et al. 2004; Lorch et al. 2011; Musladin et al. 2014). Chromatin remodelers are localized to the genome via bromodomains that recognize specific acetyl-lysine residues in histones (Xue et al. 2000; Lemon et al. 2001; Ferreira et al. 2007; Mujtaba et al. 2007; Filippakopoulos et al. 2012). PBAF is a large multisubunit ATP-dependent chromatin-remodeling complex that mobilizes and/or evicts nucleosomes to regulate key cellular processes, including transcription, DNA repair, and replication (Xue et al. 2000; Lemon et al. 2001; Kakarougkas et al. 2014). Prior biochemical and imaging studies have demonstrated that bromodomains within PBAF and its yeast counterpart, RSC, increase affinity of these remodelers for chromatin (VanDemark et al. 2007; Johnson et al. 2008; Wang et al. 2012; Duan and Smerdon 2014; Philpott et al. 2014; Porter and Dykhuizen 2017). The majority of PBAF's bromodomains (6 out of 8) are located in the BAF180 subunit of PBAF (Brownlee et al. 2012). BAF180 likely uses these six bromodomains to facilitate PBAF's localization to a large number of differentially acetylated genomic loci including regions at the 5' and 3' end of genes (Rhee and Pugh 2012). RSC has also been found to bind intergenic regions such as enhancers and insulators (Jambunathan et al. 2005; Oki and Kamakaka 2005; Lan et al. 2012). This localization function is likely clinically important due to the high rate of BAF180 mutation in certain types of cancer including clear cell renal cell carcinoma (Varela et al. 2011; Cancer

Genome Atlas Research 2013). Therefore understanding the role of the BAF180 bromodomains in recognition of acetylated genomic loci is important both clinically and to our understanding of transcription.

Once bound to chromatin, PBAF and RSC have been implicated in both activation and repression of transcription (Cairns et al. 1996; Lemon et al. 2001; Damelin et al. 2002; Van de Vosse et al. 2013; Kakarougkas et al. 2014; Nichol et al. 2016). PBAF is thought to evict nucleosomes from enhancers and promoters to potentiate transcription (Kim et al. 2009; Yen et al. 2012; Krietenstein et al. 2016; Marathe et al. 2017). In support of this model, in vivo conditional knockout of RSC leads to rapid nucleosome accumulation throughout highly transcribed genes (Parnell et al. 2008). RSC also has documented roles in transcriptional repression of the histone locus and subtelomeric genes (Van de Vosse et al. 2013), modulation of telomere length (Askree et al. 2004), and the DNA damage response (Shim et al. 2005). In addition, PBAF represses transcription of genes surrounding sites of DNA damage (Kakarougkas et al. 2014). PBAF and RSC may act to reposition nucleosomes via sliding to inhibit transcription factor binding and transcription initiation-given that nucleosome eviction is unlikely compatible with repression,

The dynamics of chromatin remodeling in vitro have suggested that swi/snf chromatin remodelers, including PBAF and RSC, utilize differing enzyme kinetics for sliding versus eviction of nucleosomes (Whitehouse et al. 1999; Boeger et al. 2003; Bruno et al. 2003; Boeger et al. 2004; Lorch et al. 2006; Lorch et al. 2011; Musladin et al. 2014; Clapier et al. 2016; Clapier et al. 2017).

At high DNA translocation efficiencies, RSC rapidly slides and ejects nucleosomes. Inefficient DNA translocation leads to slow nucleosome sliding without eviction (Clapier et al. 2016).

In vivo and in vitro attempts to measure chromatin-remodeling kinetics have so far produced different estimates. In vitro approaches suggest that chromatin remodelers require at least 10s of seconds to remodel nucleosomes (Zhang et al. 2006; Harada et al. 2016). In contrast, in vivo approaches using FRAP suggest that chromatin remodelers interact with chromatin on the order of a few seconds (Phair et al. 2004; Johnson et al. 2008; Erdel et al. 2010; Erdel and Rippe 2012; Philpott et al. 2014). This discrepancy between timescales for chromatin remodeling in vitro and in vivo could potentially be related to heterogenous interactions of remodelers and different states of chromatin. Thus additional imaging approaches are necessary to probe chromatin-remodeler function at high temporal and spatial resolution in vivo.

Single molecule imaging is a method to potentially interrogate the dynamics of chromatin remodeling within the complex milieu of the nucleus. Progress in live-cell single-particle tracking (SPT) techniques has accelerated with advances in both microscopy and fluorescent dyes (Chen et al. 2014; Izeddin et al. 2014; Liu et al. 2014; Grimm et al. 2015; Knight et al. 2015; Coleman et al. 2016; Zhen et al. 2016). This has allowed for direct in-vivo tracking of individual nuclear factors with unparalleled spatial and temporal resolution. In addition, due to the improved photochemical properties of dyes, one can now continuously image single-particle dynamics across an entire

nucleus for seconds to minutes. SPT also allows for classification of populations displaying heterogeneous chromatin binding interactions.

We have used SPT of fluorescently tagged human BAF180 to characterize PBAF's interaction with chromatin in live cells. We found that PBAF transiently and non-specifically probed chromatin on sub-second timescales. Upon stable binding to chromatin in cells, PBAF remained engaged for ~14 seconds on average, consistent with in vitro measurements (Zhang et al. 2006). Deletion of BAF180 bromodomains decreased the percentage of stable binding events and PBAF's residence time on chromatin. Furthermore, PBAF binds to chromatin in distinct subnuclear regions with different kinetics. We assessed PBAF binding activity within regions of chromatin containing high densities of H3.3 (actively transcribing) versus HP1α (repressed). Strikingly PBAF binds H3.3 regions for significantly less time than HP1α marked areas suggesting potentially high ATP-dependent nucleosome turnover within transcriptionally active regions. Furthermore, stimulation of histone acetylation, primarily leads to increased genomic localization and repeated binding of PBAF within small subnuclear foci. Accordingly, deletion of BAF180 bromodomains reduces PBAF's clustered binding in foci. Overall, our study shows how PBAF genomic localization and binding dynamics are regulated via bromodomain-acetyl-lysine interactions and select chromatin states.

Results

In vivo single particle tracking of PBAF reveals multiple bromodomain-regulated chromatin binding modes.

To characterize the dynamic binding of PBAF to chromatin *in vivo*, we created a stable U2-OS cell line expressing Halo- and flag-tagged human BAF180 (Halo-fBAF180) (Supplemental Figure S1A). Expression was confirmed through *in vivo* labeling of Halo-fBAF180 using a membrane permeable dye (JF549 conjugated Halo-Tag Ligand (JF549HTL)) followed by SDS-PAGE and comparison against a cell line expressing the Halo-tag alone (Supplementary Figure S1B). Western blotting using an antibody against BAF180 revealed that Halo-fBAF180 is overexpressed ~1.7-fold compared to control cell lines containing the Halo-tag alone (Supplementary Figure S1C). To confirm the incorporation of Halo-fBAF180 into the PBAF complex, immunoprecipitation against the flag-tag followed by western blotting against the BRG1 subunit was performed. Flag-tag immunoprecipation from Halo-fBAF180 containing lysates had significantly more BRG1 compared to Halo-alone, suggesting successful assembly of Halo-fBAF180 into the PBAF complex (Supplementary Figure S1D).

Halo-fBAF180 was fluorescently labeled in live cells using JF549HTL (Grimm et al. 2015). Live cell Single Molecule Tracking (SMT) was then performed using HILO microscopy (Figure 1A and Supplemental Movie) (Chen et al. 2014).

To determine if our Halo-fBAF180 construct was incorporated into the PBAF complex, we first conducted fast diffusion experiments by imaging Halo-fBAF180 using short camera exposure times (effective exposure time = 25 ms).

Point Spread Functions (PSFs) of single Halo-fBAF180 particles can be resolved at these exposure times even when they are freely diffusing. Multiple Target Tracking (MTT) algorithms were applied to single Halo-fBAF180 molecules (Serge et al. 2008). The trajectories of single Halo-fBAF180 molecules then had their Mean Square Displacement (MSD) calculated. This MSD was then used to calculate a diffusion coefficient (D_{coeff}) for Halo-fBAF180 particles (Figure S2). Halo-fBAF180 that isn't incorporated into PBAF should have a D_{coeff} = 3-5μm^2/sec, based on measurements of a comparable protein complex with a molecular weight similar to Halo-fBAF180 (Schmidt et al. 2016). We conclude that most of our Halo-fBAF180 is incorporated into the high molecular weight PBAF complex given that very little of our imaged Halo-fBAF180 particles possessed a D_{coeff} in this range,

To image PBAF molecules stably bound to chromatin, we utilized long camera exposures of 500 ms. Fast-diffusing molecules cannot be resolved as single particles and are blurred out at this longer exposure time. Single PBAF molecules, stably bound to chromatin targets, appear as distinct PSFs that can be spatially and temporally resolved. MTT algorithms could then be applied as above to single PBAF molecules to determine PBAF chromatin-binding activity over time throughout the nucleus. Single molecules of Halo-fBAF180 within individual frames of a movie were first localized through 2D Gaussian fitting. Chromatin-binding events were defined as a track by linking single BAF180 molecules in successive frames whose positions remained in a highly confined area based on expected diffusion constants (Figure 1B, panel i). Each

chromatin-binding event was mapped by averaging the position of all individual localizations within the entire track (Figure 1B, panel i red X). On average, 19,287 PBAF chromatin-binding events were localized in each live cell during ~18 minutes of continuous imaging (Figure 1B, panels ii and iii). The residence time of Halo-fBAF180 bound to chromatin was defined as the length in seconds of individual binding events (Figure 1C). Chromatin-binding dynamics of PBAF were then quantitatively evaluated by using a single and a two-component exponential distribution model to fit a histogram of residence times (Figure 1D)(Chen et al. 2014). A single exponential model yielded poor fits with ~2.3 second residence time, which was similar to values obtained with FRAP (Philpott et al. 2014; Gerstenberger et al. 2016). Fitting the residence time histograms with a double exponential function yielded two chromatin-binding populations of PBAF (Figure 1D). The predominant PBAF population (~86% of molecules) bound chromatin transiently with a residence time of ~0.8 seconds. Based upon previous studies, this population likely represents non-specific scanning of PBAF along the genome (Chen et al. 2014). The remaining PBAF molecules (~14%) bound chromatin stably with an average residence time of ~13.9 seconds (Figure 1E). Importantly, photobleaching rates occurred with a $t_{1/2}$ of approximately 100-200 seconds indicating that we are likely measuring PBAF's dissociation from chromatin.

Multiple PBAF subunits, including BAF180, BRG1 and BRD7, contain bromodomains that recognize acetyl-lysine residues in chromatin (Charlop-Powers et al. 2010; Ho and Crabtree 2010; Brownlee et al. 2012;

Filippakopoulos et al. 2012). To determine the contribution of bromodomains to PBAF binding, we deleted the six bromodomains within BAF180 (BAF180-ΔBD) (Supplemental Figure S1A). Deletion of BAF180 bromodomains resulted in a decrease in both the residence time (Figure 1E) and the proportion of molecules stably bound to chromatin (Supplemental Figure S3). Conversely, we wanted to determine if increased levels of lysine acetylation stabilizes PBAF binding to chromatin. Thus, cells stably expressing Halo-fBAF180 were pre-incubated with a histone deacetylase inhibitor (SAHA) for 24 hours prior to imaging. Western blotting confirmed a ~4-fold increase of histone acetylation with SAHA treatment (Supplemental Figure S4). Interestingly, no changes in residence time (Figure 1E) or in the proportion of molecules stably binding to chromatin (Supplemental Figure S3) were observed upon incubation of cells with SAHA. This suggests that increased histone acetylation doesn't globally change PBAF's chromatin-binding association or dissociation kinetics.

PBAF dynamically binds chromatin in discrete subnuclear regions

Previous studies showed that the effects of histone acetylation on transcriptional bursting dynamics are promoter specific (Suter et al. 2011). Therefore we hypothesized that only certain sub-populations of PBAF molecules interacting with select genomic loci might be differentially affected by bromodomain/acetyl-lysine interactions. We sought to dissect this heterogeneous chromatin-binding in a spatial and a temporal manner. First, we mapped out areas of high PBAF binding density (Figure 2A left). Binding density heat maps were generated by counting the number of PBAF-chromatin binding

events (binding events/μm^2/sec) in a given window (18 x 18 pixels, 2.29 μm^2) as it was raster scanned across the nucleus one pixel at a time. The heat map was then filtered to include territories containing PBAF-chromatin binding density above the global average density. Remaining territories were then further filtered to require at least 120 PBAF-chromatin binding events/territory (Figure 2A right).

Next, the residence time for PBAF molecules collectively bound within individual territories was determined. As with the global level of analysis, two populations (e.g. stable and unstable) of PBAF bound chromatin within territories emerged (Figure 2B). Strikingly, territories displayed a large degree of variability in the residence time and percentage of PBAF stably bound to chromatin (Figures 2B, 2C and Supplemental Figure S5A). In contrast, there was minimal variation in the residence time amongst the different territories for the PBAF population that was not stably bound to chromatin (Supplemental Figure S5B).

When wild type BAF180 (Halo-fBAF180WT) was examined, PBAF's residence times on chromatin within territories varied from ~2.8-42.9 seconds (Figures 2C, and data not shown). In contrast to our global analysis, a histogram of PBAF chromatin binding residence times within territories revealed two populations exhibiting average residence times of ~11.4 and 19.6 seconds (Figure 3A green curve). Elimination of BAF180 bromodomains (Halo-fBAF180-ΔBD) resulted in two populations displaying a significant decrease in PBAF's residence time on chromatin compared to wild-type BAF180 (Figure 3A red curve). Contrary to our global analysis (Figure 1E), increasing acetylation levels

via SAHA treatment of cells resulted in a slightly elevated BAF180 residence time on chromatin in territories (Figure 3B brown curve). Overall our data suggest distinct pools of PBAF target loci that are clustered in large territories throughout different subnuclear regions. PBAF's interaction with these target loci can be regulated via bromodomain-acetyl-lysine interactions with chromatin.

PBAF exhibits shorter stable chromatin binding interactions within euchromatic versus heterochromatic regions

We next sought to determine how PBAF-chromatin binding activity changes in euchromatin versus heterochromatin. To differentially localize euchromatin and heterochromatin within the cell, we conducted two-color SPT imaging with PBAF using Halo-fBAF180WT and either H3.3-SNAP or SNAP-HP1α respectively. SPT traces of H3.3-SNAP or SNAP-HP1α were isolated and used to generate high density H3.3 or HP1α territories within cells (Figures 4A top left and Supplemental Figure S6). PBAF SPT trajectories from the same cells were masked using these H3.3 or HP1α territories (Figure 4A bottom and Supplemental Figure S6 bottom). 1-CDF plots of PBAF residence times mapped within H3.3 or HP1α territories were fitted to a double-exponential function. BAF180 tracks that localized within H3.3 territories bound for a shorter duration than tracks that localized within HP1α territories (Figure 4B).

Bromodomain dependent clustering of PBAF bound to chromatin in small foci

PBAF is known to localize to small genomic regions in enhancers or at the 5' and 3' ends of genes (Yen et al. 2012; Marathe et al. 2017). Therefore, we

wanted to investigate whether PBAF bound chromatin in high-density clusters, given recent reports showing the binding of various nuclear factors and nucleosomes in restricted nuclear domains less than 250 nm [Cisse, 2013 #90;Liu, 2014 #9;Ricci, 2015 #94]. To determine if PBAF was dynamically and repeatedly sampling small genomic regions, we developed a method to generate high-resolution binding density heat maps. We increased the resolution of our analysis by reducing the size of our scanning widow ~10 fold to 168nm in diameter and then counting the number of PBAF/chromatin binding events throughout the nucleus (Figure 5A). Clustering algorithms were used to define small foci of repeated PBAF/chromatin binding events within 168nm having a minimum residence time of at least 2 seconds (Figure 5B). Further filtering revealed small foci of repeated PBAF/chromatin binding events lasting longer than 12 seconds (Figure 5C, left panel). Importantly, no clustering was detected in simulations where localizations of an equivalent number of binding events were randomized throughout the nucleus (Figure 5C, right panel).

The number of small foci detected scaled linearly based on the number of PBAF binding events in each cell (Figure 6A). This linear relationship between foci detected and number of PBAF binding events allowed comparison between cells expressing either Halo-fBAF180WT or Halo-fBAF180-ΔBD (Figure 6A). Consistent with our prior residence time and territorial data, deletion of the bromodomains within BAF180 led to deficits in PBAF clustering when filtering for binding durations as low as 2 seconds (Figure 6A). These differences were maintained when filtering for longer binding durations (Figure 6B). In contrast,

increased histone acetylation via SAHA treatment did not affect Halo-fBAF180WT PBAF clustering at a 2-second event threshold (Figure 6C). However, increased histone acetylation did result in a greater number of clusters formed at thresholds of 8 and 12-seconds relative to DMSO treatment (Figures 6D and E). This suggests that increased histone acetylation preferentially leads to repeated long-lived PBAF binding at an increased number of genomic loci. Taken together, bromodomain-acetyl-lysine interactions function to both increase targeting and anchoring of PBAF to select genomic loci.

Discussion

PBAF dynamically interacts with chromatin targets

Our live cell SPT assays reveal that PBAF/BAF180 dynamically samples the genome via a series of brief interactions (<1 second) in search of chromatin targets (Figure 1D). Removal of BAF180's bromodomains decreases the search efficiency (Figure S3) resulting in a higher percentage of transient unstable interactions with chromatin. This finding is consistent with previous studies indicating that bromodomains enhance association of remodeling complexes with chromatin (Hassan et al. 2002; Philpott et al. 2014; Porter and Dykhuizen 2017).

Once PBAF/BAF180 finds its target, it remains bound to chromatin for ~14 seconds on average throughout the nucleus. Strikingly, deletion of BAF180's bromodomains leads to a shorter chromatin binding residence time (~10 seconds-ΔBD vs 14 seconds-WT) (Figure 1E). PBAF also bound chromatin in large unique subnuclear regions displaying primarily two distinct residence times of ~11 and 19 seconds (Figures 2 and 3A). These large contiguous subnuclear regions may indicate formation of chromatin territories that must be remodeled by PBAF during regulation of transcription, replication or DNA repair (Xue et al. 2000; Lemon et al. 2001; Kakarougkas et al. 2014). Disruption of BAF180 bromodomains reduced PBAF's residence time within these large subnuclear regions to approximately 8 seconds (Figure 3A). Thus PBAF binding in these large territories is likely regulated by bromodomains that anchor the complex to acetylated nucleosomes.

Notably, the global percentage of stable chromatin binding and the residence time of PBAF were unchanged upon stimulation of histone acetylation (Figures 1E and S3). SAHA treatment did however lead to a slight but significant increase in PBAF's residence time in large subnuclear regions (Figure 3B). It is unclear if SAHA treatment increases the number of acetylations on a single nucleosome. If this were the case, our results suggests that PBAF might only interact with a subset of histone acetylation marks on a single nucleosome at any given time, despite BAF180's six bromodomains. Therefore, increasing the number of acetylation marks on a single nucleosome would have a limited effect on PBAF's residence time.

Interestingly, PBAF displays dynamic repeated binding in small foci (~250nm) (Figure 5). These binding foci may be related to PBAF's localization to nucleosomes in enhancers along with the 5' and 3' end of genes, where PBAF may act to remodel chromatin in highly localized regions during multiple rounds of transcriptional bursts (Yen et al. 2012; Marathe et al. 2017). The number of these PBAF binding foci decreases upon deletion of BAF180's bromodomains (Figure 6A). Correspondingly, the number of binding foci (i.e. clusters) containing repeated long-lived PBAF chromatin binding events increases upon SAHA treatment (Figures 6B and 7A). This suggests that SAHA treatment may lead to a greater number of acetylated nucleosomes throughout the genome. However this potential increase in acetylated nucleosomes at select sites does not shift the global chromatin binding characteristics of PBAF (Figures 1E and S4). This finding is consistent with previous work showing promoter specific effects upon

inhibition of histone deacetylase activity (Huang et al. 2014; Rafehi et al. 2014; Vleeshouwer-Neumann et al. 2015). Overall, we envision that histone deacetylation reduces both targeting of PBAF to chromatin and the duration of stable binding at specific genomic loci in vivo (Figure 7A).

PBAF interaction dynamics in euchromatic versus heterochromatic regions

Previous studies documented that actively transcribing genes in euchromatin display dynamic chromatin incorporation and turnover of H3.3 relative to heterochromatic regions (Deaton et al. 2016). In addition, in vitro experiments revealed that H3.3 containing nucleosomes are particularly sensitive to salt and therefore inherently unstable (Jin and Felsenfeld 2007; Henikoff et al. 2009; Jin et al. 2009). Thus it is likely that chromatin remodelers would require less time to remodel and evict H3.3 containing nucleosomes than heterochromatin lacking H3.3. Indeed our two color imaging experiments revealed that PBAF displayed shorter residence times in H3.3 marked actively transcribing regions compared to HP1α containing heterochromatic regions (Figures 4B and 7B). Therefore rapid turnover of PBAF's genomic occupancy in actively transcribing regions could be the direct result of nucleosome stability, which may define different chromatin states.

These results (Figure 4B) may seem contradictory to our experiments showing slightly longer lived PBAF residence times upon increased acetylation (Figure 3B), given that actively transcribed regions are associated with high levels of acetylation. However, we speculate that this is due to intrinsic differences between nucleosomes in actively transcribed regions versus other

acetylated regions of the genome. As previously described, nucleosomes in actively transcribing euchromatin also contain histone variants and are enriched in histone post-translational modifications within the histone globular region that favor destabilization or eviction of nucleosomes (Ahmad and Henikoff 2002; Di Cerbo et al. 2014; Bowman and Poirier 2015; Deaton et al. 2016; Pradhan et al. 2016). This likely results in the short-lived PBAF residence times observed in H3.3-rich nuclear regions. Strikingly however, most PBAF binding events still occur outside of H3.3-rich regions and thus are not in areas of active transcription. Following SAHA treatment however, it is possible that there is a selective enrichment in acetylation of residues that favor nucleosome repositioning (i.e. N-terminal histone tails) rather than those that favor nucleosome destabilization (i.e. histone globular domain) (Bowman and Poirier 2015). Indeed, SAHA preferentially lead to increases in acetylation of histone N-terminal residues, without increased acetylation of the more globular lysine residue H3K56 (Drogaris et al. 2012). Thus it is possible that inhibition of histone deacetylase activity with SAHA enhances PBAF localization to this new more stable pool of nucleosome particles. PBAF localization to these stable nucleosomes could be related to other roles for PBAF outside of transcription such as repression, DNA repair, and specification of pericentromeric or subtelomeric regions (Ferreira et al. 2011; Verdaasdonk et al. 2012; Van de Vosse et al. 2013; Kakarougkas et al. 2014)

PBAF's chromatin binding in relation to nucleosome remodeling kinetics and transcriptional bursting dynamics

PBAF and RSC are thought to remodel nucleosomes via DNA translocation (Velankar et al. 1999; Zhang et al. 2006; Clapier et al. 2016; Clapier et al. 2017). Interestingly, in vitro single molecule studies on RSC have revealed that the average duration for nucleosomal DNA translocation is ~10 seconds (Zhang et al. 2006). Roughly equivalent timescales between in vitro DNA translocation and in vivo chromatin residence time (~11-14 seconds, Figures 1E and 3A), suggests that we may be visualizing nucleosome remodeling in our live-cell single molecule studies. However at this time, we cannot determine if PBAF is evicting or sliding nucleosomes in our imaging experiments. High-resolution live-cell two color imaging of PBAF bound to fluorescently tagged nucleosomes will help delineate these possibilities.

PBAF's residence time on chromatin is highly similar to an activator (Sox2, ~15 seconds (Chen et al. 2014)) and the Polycomb repressor (Cbx7, ~7 seconds (Zhen et al. 2016)) as measured using single particle tracking. This further indicates that a variety of transcription factors dynamically access their chromatin targets on timescales of seconds. RNA Pol II recruitment and promoter escape also occurs approximately every 4-8 seconds during transcriptional bursts (Tantale et al. 2016). Therefore the fast dynamics of transcriptional bursts likely necessitates rapid binding and unbinding of transcriptional regulators such as chromatin remodelers, activators, and repressors.

Materials and Methods

Plasmid constructions and biochemistry

Details of plasmid construction and biochemical analysis of Halo-BAF180 can be found in the supplemental methods section.

Cell Culture and generation of FRT site, Halo-tag, Halo-fBAF180WT, Halo-fBAF180WT/SNAP-HP1α, and Halo-fBAF180WT/H3.3-SNAP stable cell lines

U2-OS cells were grown in complete DMEM (high glucose DMEM supplemented with 10% FBS, 2 mM Glutamax (Fisher Scientific), 100 I.U./mL Penicillin, and 100 ug/mL Streptomycin (Corning)). To create U2-OS cells containing a single FRT site for future generation of isogenic cell lines, we transiently transfected cells with pFRT/lacZeo plasmid containing an FRT site (Invitrogen). Single cell colonies were selected in 300 ug/mL zeocin. To create the Halo-tag or Halo-fBAF180WT cell lines, pFRT-Halo or pFRT-Halo-fBAF180WT plasmids were co-transfected with pOG44 plasmid into U2-OS-FRT cells. Selection for Halo-tag or Halo-fBAF180WT stably expressing cells was performed by supplementing media with 75-150 ug/mL Hygromycin b. To create Halo-fBAF180WT/SNAP-HP1α or Halo-fBAF180WT/H3.3-SNAP stable cells lines, cells stably expressing Halo-fBAF180WT were co-transfected with pSNAP-HP1α or pSNAP-H3.3 plasmids together with a second plasmid containing puromycin resistance. Cells expressing Halo-fBAF180WT along with SNAP-HP1α or H3.3-SNAP were selected using puromycin.

Live-cell fluorescent labeling of Halo-fBAF180 WT and Halo-fBAF180-Δ BD in U2-OS cells

Cells stably expressing Halo-fBAF180WT were plated on 35 mm MatTek imaging dishes 2-3 days before imaging in selective media so that on the day of imaging, there would be ~5x10^5 cells/imaging dish. In the case of Halo-fBAF180-ΔBD, 24 hours prior to transfection, parental U2-OS cell were plated in 35mm MatTek imaging dishes at a density of 5x10^4 cells/imaging dish. Cells were then transiently transfected with the pFRT-Halo-BAF180-ΔBD plasmid 17-20 hours later. Following transfection, cells were incubated overnight.

24 hours before labeling, cells were treated with either 2.5 uM SAHA or matching vehicle control (DMSO 0.25% final volume) and were incubated at 37°C with 5% CO_2. Immediately prior to imaging, cells were incubated with 0.4 nM JF549-HTL for 15 minutes at 37°C with 5% CO_2. Cells were then washed 3x with 1x PBS and placed in complete DMEM and incubated for 30 minutes at 37°C with 5% CO_2. Cells were then washed 2x with 1x PBS and placed in L-15 imaging media + 10% FBS for imaging. All labeling and imaging was conducted in the presence of either 2.5 uM SAHA or DMSO.

Dual color live-cell fluorescent labeling of Halo-fBAF180WT and SNAP-HP1 α or H3.3-SNAP in U2-OS cells

Cells stably expressing Halo-fBAF180WT and either SNAP-HP1 or H3.3-SNAP were plated on 35 mm MatTek imaging dishes in selective media 1-3 days before imaging so that on the day of imaging, there would be ~5x10^5

cells/imaging dish. Immediately prior to imaging, cells were incubated at 37°C with 5% CO_2 with 10nM SNAP-Cell 647-SiR (New England Biolabs) and 0.4nm JF549-HTL for a total of 30 and 15 minutes respectively. Cells were then washed 3x with 1x PBS and placed in complete DMEM and incubated for 30 minutes at 37°C with 5% CO_2. Cells were then washed 2x with 1x PBS and placed in L-15 imaging media + 10% FBS for imaging.

Live-cell single molecule imaging of Halo-fBAF180WT, SNAP-HP1 α or H3.3-SNAP in U2-OS cells

All imaging sessions were carried out at room temperature. Samples were continuously illuminated using a 532nm (Coherent) or 640nm (Coherent) laser. Time-lapse two dimensional images of single molecules were acquired with a customized inverted Nikon Eclipse Ti microscope with a 100x oil-immersion objective lens (Nikon, 1.49NA) and further magnified 1.5x post-objective. BAF180 images were acquired at 2Hz for ~18 minutes using an EMCCD (iXon, Andor) with a 512 x 512 pixel field of view (final pixel size of 84nm). SNAP imaging proceeded at 2Hz for ~4.5 minutes in cells that also expressed either H3.3-SNAP or SNAP-HP1α.

Image Processing and single particle tracking

Acquired images were processed to subtract background and subjected to Multi-Target Tracking (MTT) to resolve the trajectories of individual molecules (Serge et al. 2008) using custom MATLAB scripts.

Determination of BAF180 chromatin binding residence times

Each cell had the nucleus masked based on boundaries of the strong nuclear BAF180 signal and confirmed via imaging using white light. Tracks that fell outside of the nucleus were excluded. Photobleach rates were then determined for each background-subtracted movie. Track-length was plotted as a 1-Cumulative Density Function (1-CDF). Single- and double-exponential models were then fitted to these 1-CDF functions to determine the residence times.

Global comparisons of stable residence times (>1 second) and proportions of molecules participating in stable residence events were conducted by taking the global stable residence time and the proportion of molecules participating in stable residence events for each cell. One-way ANOVA followed by Tukey's post-hoc t-tests were then performed to determine pairwise significance.

Mapping of PBAF binding territories

Contiguous areas of high PBAF binding density in cells were determined by 1-pixel raster scanning of an 18x18 pixel window across cells. Binding events that fell within these windows were then counted to provide an overall binding density for individual pixels throughout the nucleus. The resulting PBAF density map was then filtered so that pixels that displayed a binding density lower than the average global binding density were eliminated. Remaining areas were grouped as contiguous territories and total event number was evaluated in each region. Territories with fewer than 120 binding events were eliminated to make statistical analysis of events within territories more robust. Track lengths for

particles within remaining territories were then evaluated as 1-CDF functions and were fit to single- and double-exponential functions.

Specific binding components for each territory were plotted as Probability Density Functions (PDF) based on genotype or treatment condition. Statistical differences between treatment groups were then assessed using a two-sample Kolmogorov-Smirnov test.

Determination of territorial binding dynamics for PBAF within HP1α or H3.3 territories

High binding density HP1α or H3.3 territories were mapped using MTT and raster scanning as described above. Remaining territories were then filtered so that regions below a threshold of 0.5% of total cellular binding events for HP1α or H3.3 were eliminated. PBAF binding events within individual HP1α or H3.3 territories were then examined. Regions containing less than 120 PBAF binding events were eliminated. 1-CDF plots of PBAF binding event residence times within individual remaining territories were fitted with single- and double-exponential functions. Comparisons between PBAF populations localizing within particular territories were made using a two-sample Kolmogorov-Smirnov test.

Analysis of PBAF clustering

Event density maps were taken and rendered at a pixel size of 8.4 nm before being 1 pixel raster scanned across the nucleus with an octagon of 168 nm in diameter. Octagon widows centered on an individual pixel containing 3 PBAF binding events were considered clusters. Further filtering was conducted based

on duration of binding events lasting at least 0, 1, 2, 4, 6, 8, 10, 12, 14, or 16 seconds. For each condition, cluster number per cell was then plotted against total track number. The slope and R^2-value of the resulting regression line was calculated in each condition. Simulations were performed using randomized positions of nuclear tracks followed by clustering analysis.

Acknowledgements

We thank Y.J. Chen and C.S. Peng for development of initial Matlab scripts used for SPT tracking. We are grateful to Z. Liu for providing the Matlab script and technical advice for analysis of diffusion rates. We thank S. Healton for reagents and technical assistance in acid extraction of histones, and J.C. Wheat for providing SAHA reagent and initial aliquots of acetyl-H3 antibody. We also thank D. Shechter for providing histone H3 antibody. This work was supported by a grant from the NIH/NIBIB (1U01EB021236-03, RAC and RHS) and a NIH Medical Scientist Training Program Grant (T32GM007288, CAK).

References

Ahmad K, Henikoff S. 2002. The histone variant H3.3 marks active chromatin by replication-independent nucleosome assembly. *Mol Cell* **9**: 1191-1200.

Askree SH, Yehuda T, Smolikov S, Gurevich R, Hawk J, Coker C, Krauskopf A, Kupiec M, McEachern MJ. 2004. A genome-wide screen for Saccharomyces cerevisiae deletion mutants that affect telomere length. *Proc Natl Acad Sci U S A* **101**: 8658-8663.

Boeger H, Griesenbeck J, Strattan JS, Kornberg RD. 2003. Nucleosomes unfold completely at a transcriptionally active promoter. *Mol Cell* **11**: 1587-1598.

-. 2004. Removal of promoter nucleosomes by disassembly rather than sliding in vivo. *Mol Cell* **14**: 667-673.

Bowman GD, Poirier MG. 2015. Post-translational modifications of histones that influence nucleosome dynamics. *Chem Rev* **115**: 2274-2295.

Brownlee PM, Chambers AL, Oliver AW, Downs JA. 2012. Cancer and the bromodomains of BAF180. *Biochem Soc Trans* **40**: 364-369.

Bruno M, Flaus A, Stockdale C, Rencurel C, Ferreira H, Owen-Hughes T. 2003. Histone H2A/H2B dimer exchange by ATP-dependent chromatin remodeling activities. *Mol Cell* **12**: 1599-1606.

Cairns BR, Lorch Y, Li Y, Zhang M, Lacomis L, Erdjument-Bromage H, Tempst P, Du J, Laurent B, Kornberg RD. 1996. RSC, an essential, abundant chromatin-remodeling complex. *Cell* **87**: 1249-1260.

Calo E, Wysocka J. 2013. Modification of enhancer chromatin: what, how, and why? *Mol Cell* **49**: 825-837.

Cancer Genome Atlas Research N. 2013. Comprehensive molecular characterization of clear cell renal cell carcinoma. *Nature* **499**: 43-49.

Charlop-Powers Z, Zeng L, Zhang Q, Zhou MM. 2010. Structural insights into selective histone H3 recognition by the human Polybromo bromodomain 2. *Cell Res* **20**: 529-538.

Chen J, Zhang Z, Li L, Chen BC, Revyakin A, Hajj B, Legant W, Dahan M, Lionnet T, Betzig E et al. 2014. Single-molecule dynamics of enhanceosome assembly in embryonic stem cells. *Cell* **156**: 1274-1285.

Clapier CR, Iwasa J, Cairns BR, Peterson CL. 2017. Mechanisms of action and regulation of ATP-dependent chromatin-remodelling complexes. *Nat Rev Mol Cell Biol*.

Clapier CR, Kasten MM, Parnell TJ, Viswanathan R, Szerlong H, Sirinakis G, Zhang Y, Cairns BR. 2016. Regulation of DNA Translocation Efficiency within the Chromatin Remodeler RSC/Sth1 Potentiates Nucleosome Sliding and Ejection. *Mol Cell* **62**: 453-461.

Coleman RA, Liu Z, Darzacq X, Tjian R, Singer RH, Lionnet T. 2016. Imaging Transcription: Past, Present, and Future. *Cold Spring Harbor symposia on quantitative biology*.

Damelin M, Simon I, Moy TI, Wilson B, Komili S, Tempst P, Roth FP, Young RA, Cairns BR, Silver PA. 2002. The genome-wide localization of Rsc9, a component of the RSC chromatin-remodeling complex, changes in response to stress. *Mol Cell* **9**: 563-573.

Deaton AM, Gomez-Rodriguez M, Mieczkowski J, Tolstorukov MY, Kundu S, Sadreyev RI, Jansen LE, Kingston RE. 2016. Enhancer regions show high histone H3.3 turnover that changes during differentiation. *Elife* **5**.

Di Cerbo V, Mohn F, Ryan DP, Montellier E, Kacem S, Tropberger P, Kallis E, Holzner M, Hoerner L, Feldmann A et al. 2014. Acetylation of histone H3 at lysine 64 regulates nucleosome dynamics and facilitates transcription. *Elife* **3**: e01632.

Drogaris P, Villeneuve V, Pomies C, Lee EH, Bourdeau V, Bonneil E, Ferbeyre G, Verreault A, Thibault P. 2012. Histone deacetylase inhibitors globally enhance h3/h4 tail acetylation without affecting h3 lysine 56 acetylation. *Sci Rep* **2**: 220.

Duan MR, Smerdon MJ. 2014. Histone H3 lysine 14 (H3K14) acetylation facilitates DNA repair in a positioned nucleosome by stabilizing the binding of the chromatin Remodeler RSC (Remodels Structure of Chromatin). *J Biol Chem* **289**: 8353-8363.

Erdel F, Rippe K. 2012. Quantifying transient binding of ISWI chromatin remodelers in living cells by pixel-wise photobleaching profile evolution analysis. *Proc Natl Acad Sci U S A* **109**: E3221-3230.

Erdel F, Schubert T, Marth C, Langst G, Rippe K. 2010. Human ISWI chromatin-remodeling complexes sample nucleosomes via transient binding reactions and become immobilized at active sites. *Proc Natl Acad Sci U S A* **107**: 19873-19878.

Ferreira H, Flaus A, Owen-Hughes T. 2007. Histone modifications influence the action of Snf2 family remodelling enzymes by different mechanisms. *J Mol Biol* **374**: 563-579.

Ferreira ME, Flaherty K, Prochasson P. 2011. The Saccharomyces cerevisiae histone chaperone Rtt106 mediates the cell cycle recruitment of SWI/SNF and RSC to the HIR-dependent histone genes. *PLoS One* **6**: e21113.

Filippakopoulos P, Picaud S, Mangos M, Keates T, Lambert JP, Barsyte-Lovejoy D, Felletar I, Volkmer R, Muller S, Pawson T et al. 2012. Histone recognition and large-scale structural analysis of the human bromodomain family. *Cell* **149**: 214-231.

Gerstenberger BS, Trzupek JD, Tallant C, Fedorov O, Filippakopoulos P, Brennan PE, Fedele V, Martin S, Picaud S, Rogers C et al. 2016. Identification of a Chemical Probe for Family VIII Bromodomains through Optimization of a Fragment Hit. *J Med Chem* **59**: 4800-4811.

Grimm JB, English BP, Chen J, Slaughter JP, Zhang Z, Revyakin A, Patel R, Macklin JJ, Normanno D, Singer RH et al. 2015. A general method to improve fluorophores for live-cell and single-molecule microscopy. *Nat Methods* **12**: 244-250, 243 p following 250.

Harada BT, Hwang WL, Deindl S, Chatterjee N, Bartholomew B, Zhuang X. 2016. Stepwise nucleosome translocation by RSC remodeling complexes. *Elife* **5**.

Hassan AH, Prochasson P, Neely KE, Galasinski SC, Chandy M, Carrozza MJ, Workman JL. 2002. Function and selectivity of bromodomains in anchoring chromatin-modifying complexes to promoter nucleosomes. *Cell* **111**: 369-379.

Hebbes TR, Allen SC. 2000. Multiple histone acetyltransferases are associated with a chicken erythrocyte chromatin fraction enriched in active genes. *J Biol Chem* **275**: 31347-31352.

Henikoff S, Henikoff JG, Sakai A, Loeb GB, Ahmad K. 2009. Genome-wide profiling of salt fractions maps physical properties of chromatin. *Genome Res* **19**: 460-469.

Ho L, Crabtree GR. 2010. Chromatin remodelling during development. *Nature* **463**: 474-484.

Huang J, Schriefer AE, Yang W, Cliften PF, Rudnick DA. 2014. Identification of an epigenetic signature of early mouse liver regeneration that is disrupted by Zn-HDAC inhibition. *Epigenetics* **9**: 1521-1531.

Izeddin I, Recamier V, Bosanac L, Cisse, II, Boudarene L, Dugast-Darzacq C, Proux F, Benichou O, Voituriez R, Bensaude O et al. 2014. Single-molecule tracking in live cells reveals distinct target-search strategies of transcription factors in the nucleus. *eLife* **3**.

Jambunathan N, Martinez AW, Robert EC, Agochukwu NB, Ibos ME, Dugas SL, Donze D. 2005. Multiple bromodomain genes are involved in restricting the spread of heterochromatic silencing at the Saccharomyces cerevisiae HMR-tRNA boundary. *Genetics* **171**: 913-922.

Jenuwein T, Allis CD. 2001. Translating the histone code. *Science* **293**: 1074-1080.

Jin C, Felsenfeld G. 2007. Nucleosome stability mediated by histone variants H3.3 and H2A.Z. *Genes Dev* **21**: 1519-1529.

Jin C, Zang C, Wei G, Cui K, Peng W, Zhao K, Felsenfeld G. 2009. H3.3/H2A.Z double variant-containing nucleosomes mark 'nucleosome-free regions' of active promoters and other regulatory regions. *Nat Genet* **41**: 941-945.

Johnson TA, Elbi C, Parekh BS, Hager GL, John S. 2008. Chromatin remodeling complexes interact dynamically with a glucocorticoid receptor-regulated promoter. *Molecular biology of the cell* **19**: 3308-3322.

Kakarougkas A, Ismail A, Chambers AL, Riballo E, Herbert AD, Kunzel J, Lobrich M, Jeggo PA, Downs JA. 2014. Requirement for PBAF in transcriptional repression and repair at DNA breaks in actively transcribed regions of chromatin. *Mol Cell* **55**: 723-732.

Kim SI, Bresnick EH, Bultman SJ. 2009. BRG1 directly regulates nucleosome structure and chromatin looping of the alpha globin locus to activate transcription. *Nucleic Acids Res* **37**: 6019-6027.

Knight SC, Xie L, Deng W, Guglielmi B, Witkowsky LB, Bosanac L, Zhang ET, El Beheiry M, Masson JB, Dahan M et al. 2015. Dynamics of CRISPR-Cas9 genome interrogation in living cells. *Science* **350**: 823-826.

Krietenstein N, Wal M, Watanabe S, Park B, Peterson CL, Pugh BF, Korber P. 2016. Genomic Nucleosome Organization Reconstituted with Pure Proteins. *Cell* **167**: 709-721 e712.

Lan X, Witt H, Katsumura K, Ye Z, Wang Q, Bresnick EH, Farnham PJ, Jin VX. 2012. Integration of Hi-C and ChIP-seq data reveals distinct types of chromatin linkages. *Nucleic Acids Res* **40**: 7690-7704.

Larson DR, Zenklusen D, Wu B, Chao JA, Singer RH. 2011. Real-time observation of transcription initiation and elongation on an endogenous yeast gene. *Science* **332**: 475-478.

Lemon B, Inouye C, King DS, Tjian R. 2001. Selectivity of chromatin-remodelling cofactors for ligand-activated transcription. *Nature* **414**: 924-928.

Liu Z, Legant WR, Chen BC, Li L, Grimm JB, Lavis LD, Betzig E, Tjian R. 2014. 3D imaging of Sox2 enhancer clusters in embryonic stem cells. *eLife* **3**: e04236.

Lorch Y, Griesenbeck J, Boeger H, Maier-Davis B, Kornberg RD. 2011. Selective removal of promoter nucleosomes by the RSC chromatin-remodeling complex. *Nat Struct Mol Biol* **18**: 881-885.

Lorch Y, Maier-Davis B, Kornberg RD. 2006. Chromatin remodeling by nucleosome disassembly in vitro. *Proc Natl Acad Sci U S A* **103**: 3090-3093.

Marathe HG, Watkins-Chow DE, Weider M, Hoffmann A, Mehta G, Trivedi A, Aras S, Basuroy T, Mehrotra A, Bennett DC et al. 2017. BRG1 interacts with SOX10 to establish the melanocyte lineage and to promote differentiation. *Nucleic Acids Res*.

Metivier R, Penot G, Hubner MR, Reid G, Brand H, Kos M, Gannon F. 2003. Estrogen receptor-alpha directs ordered, cyclical, and combinatorial recruitment of cofactors on a natural target promoter. *Cell* **115**: 751-763.

Mujtaba S, Zeng L, Zhou MM. 2007. Structure and acetyl-lysine recognition of the bromodomain. *Oncogene* **26**: 5521-5527.

Musladin S, Krietenstein N, Korber P, Barbaric S. 2014. The RSC chromatin remodeling complex has a crucial role in the complete remodeler set for yeast PHO5 promoter opening. *Nucleic Acids Res* **42**: 4270-4282.

Nichol JN, Galbraith MD, Kleinman CL, Espinosa JM, Miller WH, Jr. 2016. NPM and BRG1 Mediate Transcriptional Resistance to Retinoic Acid in Acute Promyelocytic Leukemia. *Cell Rep* **14**: 2938-2949.

Oki M, Kamakaka RT. 2005. Barrier function at HMR. *Mol Cell* **19**: 707-716.

Parnell TJ, Huff JT, Cairns BR. 2008. RSC regulates nucleosome positioning at Pol II genes and density at Pol III genes. *EMBO J* **27**: 100-110.

Phair RD, Scaffidi P, Elbi C, Vecerova J, Dey A, Ozato K, Brown DT, Hager G, Bustin M, Misteli T. 2004. Global nature of dynamic protein-chromatin

interactions in vivo: three-dimensional genome scanning and dynamic interaction networks of chromatin proteins. *Mol Cell Biol* **24**: 6393-6402.

Philpott M, Rogers CM, Yapp C, Wells C, Lambert JP, Strain-Damerell C, Burgess-Brown NA, Gingras AC, Knapp S, Muller S. 2014. Assessing cellular efficacy of bromodomain inhibitors using fluorescence recovery after photobleaching. *Epigenetics Chromatin* **7**: 14.

Porter EG, Dykhuizen EC. 2017. Individual Bromodomains of Polybromo-1 Contribute to Chromatin Association and Tumor Suppression in Clear Cell Renal Carcinoma. *J Biol Chem* **292**: 2601-2610.

Pradhan SK, Su T, Yen L, Jacquet K, Huang C, Cote J, Kurdistani SK, Carey MF. 2016. EP400 Deposits H3.3 into Promoters and Enhancers during Gene Activation. *Mol Cell* **61**: 27-38.

Rafehi H, Balcerczyk A, Lunke S, Kaspi A, Ziemann M, Kn H, Okabe J, Khurana I, Ooi J, Khan AW et al. 2014. Vascular histone deacetylation by pharmacological HDAC inhibition. *Genome Res* **24**: 1271-1284.

Raser JM, O'Shea EK. 2004. Control of stochasticity in eukaryotic gene expression. *Science* **304**: 1811-1814.

Rhee HS, Pugh BF. 2012. ChIP-exo method for identifying genomic location of DNA-binding proteins with near-single-nucleotide accuracy. *Curr Protoc Mol Biol* **Chapter 21**: Unit 21 24.

Sanchez A, Choubey S, Kondev J. 2013. Regulation of noise in gene expression. *Annu Rev Biophys* **42**: 469-491.

Sanchez A, Golding I. 2013. Genetic determinants and cellular constraints in noisy gene expression. *Science* **342**: 1188-1193.

Schmidt JC, Zaug AJ, Cech TR. 2016. Live Cell Imaging Reveals the Dynamics of Telomerase Recruitment to Telomeres. *Cell* **166**: 1188-1197 e1189.

Senecal A, Munsky B, Proux F, Ly N, Braye FE, Zimmer C, Mueller F, Darzacq X. 2014. Transcription factors modulate c-Fos transcriptional bursts. *Cell Rep* **8**: 75-83.

Serge A, Bertaux N, Rigneault H, Marguet D. 2008. Dynamic multiple-target tracing to probe spatiotemporal cartography of cell membranes. *Nat Methods* **5**: 687-694.

Shim EY, Ma JL, Oum JH, Yanez Y, Lee SE. 2005. The yeast chromatin remodeler RSC complex facilitates end joining repair of DNA double-strand breaks. *Mol Cell Biol* **25**: 3934-3944.

Sun JM, Chen HY, Espino PS, Davie JR. 2007. Phosphorylated serine 28 of histone H3 is associated with destabilized nucleosomes in transcribed chromatin. *Nucleic Acids Res* **35**: 6640-6647.

Suter DM, Molina N, Gatfield D, Schneider K, Schibler U, Naef F. 2011. Mammalian genes are transcribed with widely different bursting kinetics. *Science* **332**: 472-474.

Tantale K, Mueller F, Kozulic-Pirher A, Lesne A, Victor JM, Robert MC, Capozi S, Chouaib R, Backer V, Mateos-Langerak J et al. 2016. A single-molecule

view of transcription reveals convoys of RNA polymerases and multi-scale bursting. *Nat Commun* **7**: 12248.

Tirosh I, Barkai N. 2008. Two strategies for gene regulation by promoter nucleosomes. *Genome Res* **18**: 1084-1091.

Tirosh I, Barkai N, Verstrepen KJ. 2009. Promoter architecture and the evolvability of gene expression. *J Biol* **8**: 95.

Van de Vosse DW, Wan Y, Lapetina DL, Chen WM, Chiang JH, Aitchison JD, Wozniak RW. 2013. A role for the nucleoporin Nup170p in chromatin structure and gene silencing. *Cell* **152**: 969-983.

VanDemark AP, Kasten MM, Ferris E, Heroux A, Hill CP, Cairns BR. 2007. Autoregulation of the rsc4 tandem bromodomain by gcn5 acetylation. *Mol Cell* **27**: 817-828.

Varela I, Tarpey P, Raine K, Huang D, Ong CK, Stephens P, Davies H, Jones D, Lin ML, Teague J et al. 2011. Exome sequencing identifies frequent mutation of the SWI/SNF complex gene PBRM1 in renal carcinoma. *Nature* **469**: 539-542.

Velankar SS, Soultanas P, Dillingham MS, Subramanya HS, Wigley DB. 1999. Crystal structures of complexes of PcrA DNA helicase with a DNA substrate indicate an inchworm mechanism. *Cell* **97**: 75-84.

Verdaasdonk JS, Gardner R, Stephens AD, Yeh E, Bloom K. 2012. Tension-dependent nucleosome remodeling at the pericentromere in yeast. *Mol Biol Cell* **23**: 2560-2570.

Vleeshouwer-Neumann T, Phelps M, Bammler TK, MacDonald JW, Jenkins I, Chen EY. 2015. Histone Deacetylase Inhibitors Antagonize Distinct Pathways to Suppress Tumorigenesis of Embryonal Rhabdomyosarcoma. *PLoS One* **10**: e0144320.

Wang Y, Kallgren SP, Reddy BD, Kuntz K, Lopez-Maury L, Thompson J, Watt S, Ma C, Hou H, Shi Y et al. 2012. Histone H3 lysine 14 acetylation is required for activation of a DNA damage checkpoint in fission yeast. *J Biol Chem* **287**: 4386-4393.

Whitehouse I, Flaus A, Cairns BR, White MF, Workman JL, Owen-Hughes T. 1999. Nucleosome mobilization catalysed by the yeast SWI/SNF complex. *Nature* **400**: 784-787.

Xue Y, Canman JC, Lee CS, Nie Z, Yang D, Moreno GT, Young MK, Salmon ED, Wang W. 2000. The human SWI/SNF-B chromatin-remodeling complex is related to yeast rsc and localizes at kinetochores of mitotic chromosomes. *Proc Natl Acad Sci U S A* **97**: 13015-13020.

Yen K, Vinayachandran V, Batta K, Koerber RT, Pugh BF. 2012. Genome-wide nucleosome specificity and directionality of chromatin remodelers. *Cell* **149**: 1461-1473.

Zhang Y, Smith CL, Saha A, Grill SW, Mihardja S, Smith SB, Cairns BR, Peterson CL, Bustamante C. 2006. DNA translocation and loop formation mechanism of chromatin remodeling by SWI/SNF and RSC. *Mol Cell* **24**: 559-568.

Zhen CY, Tatavosian R, Huynh TN, Duc HN, Das R, Kokotovic M, Grimm JB, Lavis LD, Lee J, Mejia FJ et al. 2016. Live-cell single-molecule tracking reveals co-recognition of H3K27me3 and DNA targets polycomb Cbx7-PRC1 to chromatin. *Elife* **5**.

Figure Legends

Figure 1: Spatial and temporal analysis of global PBAF chromatin binding events using SPT. A. PBAF localization events within the nucleus of a U2-OS cell stably expressing Halo-fBAF180WT. Nuclear envelope is outlined in yellow. Scale bar = 2 μm. B. i. Particle centroid location was determined for each frame in the movie. Particles were temporally linked based on constrained diffusion parameters. Centroid location (red X) was determined as the mean of x- and y-positions. Scalebar = 100 nm. ii-iii. Centroid positions for each particle were mapped within the nucleus. Scalebars = 1 μm in ii and 2 μm in iii. C. Spatial positions of tracks are plotted in 2D with residence times (color-coded based on duration) for each track plotted in the third dimension. D. 1−Cumulative Distribution Function Plots (1−CDF) of PBAF bound to chromatin were fitted to a single (gray dashed) or two-component (red solid) exponential decay model. Fitting analysis reveals that PBAF bound to chromatin display two populations (stable and unstable) of residence times. Percentages of the stable and unstable binding populations are listed next to the residence time. E. Mean stable residence times are displayed for cells expressing either wild-type or bromodomain deleted Halo-fBAF180 constructs following treatment with 2.5 uM SAHA (N = 37 WT cells and 26 ΔBD cells) or vehicle control (N = 30 WT cells and 17 ΔBD cells) for 24 hours. ****= p-value < 0.0001, n.s.= not significant.

Figure 2: High density heat maps of PBAF chromatin binding events. A. Cell nuclei were mapped based on PBAF binding density (left) with regions of high PBAF binding density in red and regions of low PBAF binding density in blue. Areas of above average PBAF binding density were masked (right). B. Representative 1-CDF plots of residence times for molecules within individual masked regions from panel A (right) were fitted with

single (gray dashed) and double (red solid) -exponential functions. C. Stable binding residence times across all territories in representative cell displayed in A

Figure 3: Residence time analysis of individual high-density PBAF chromatin binding regions. A. Stable territorial PBAF residence times for wild-type BAF180 containing PBAF (white bars) and BAF180-ΔBD (gray bars). Gaussian fits of wild-type BAF180 containing PBAF (green line) and BAF180-ΔBD (red line) are provided as well. BAF180WT measurements examined 473 territories in 30 cells, while BAF180-ΔBD measurements examined 174 territories in 17 cells. B. Stable territorial PBAF residence times for wild-type BAF180 containing PBAF in cells that have been treated with 2.5 μM SAHA for 24 hours (gray bars) versus vehicle control (white bars). Gaussian fits for cells treated with SAHA (brown line) versus cells treated with vehicle (pink line) are provided as well. Effects of SAHA treatment were assessed from 571 territories in 37 cells and corresponding vehicle treatment was assessed from 473 territories in 30 cells. Vehicle data shown in B is the same as WT vehicle data shown in A of this figure.

Figure 4: Residence time analysis of PBAF binding within H3.3 marked euchromatin versus HP1α marked heterochromatin. A. Cell nuclei were mapped based on H3.3 binding density. Areas of above average H3.3 binding density within the cell were masked (top left, orange). In addition, PBAF binding events within the same cell (top right panel and bottom panel red spots), were mapped within H3.3 territories (bottom, panel orange). B. Stable PBAF residence times within H3.3 (white bars)/HP1α (black bars) territories. Gaussian fits of PBAF binding events within H3.3 (white line) or HP1α (black line) are provided. H3.3 data was amassed from 144 territories within 16 cells and HP1α was amassed from 114 territories within 16 cells.

Figure 5: Clustering analysis of PBAF chromatin binding events. A. PBAF binding density when rastering a 2x2-pixel box across the nucleus. Increased resolution reveals areas of higher PBAF binding density relative to rastering with an 18x18-pixel box as in Figure 2. B. Global WT PBAF chromatin binding maps were filtered based on duration of binding. Chromatin binding events lasting longer than 2 seconds are shown (red dots). Clustering analysis algorithms revealed repeated PBAF binding events within small foci outlined in blue. Bottom right: Expanded inset of boxed region in top panel demonstrating clustering of PBAF binding events (red dots) within clusters (blue lines). C. Global WT PBAF chromatin binding maps were filtered based on duration of binding. Chromatin binding events lasting longer than 12 seconds are shown (Top left panel, red dots). Simulated PBAF chromatin binding maps (Top right panel, red dots) were generated by randomizing the positions of the filtered binding events within the nucleus. Clustering analysis algorithms revealed repeated PBAF binding events within small foci outlined in blue. Bottom panels: Expanded insets of boxed regions in top panels demonstrating clustering of PBAF binding events (red) within clusters (blue lines).

Figure 6: Analysis of acetylation and bromodomain dependent clustering of PBAF binding to chromatin. A-B. Linear regression of wild-type (blue points and line) or bromodomain deleted (red points and line) BAF180 containing PBAF clusters versus total PBAF tracks at 2- (A) or 8-second (B) event duration filters. C-E. Linear regressions for wild-type BAF180 containing PBAF versus total PBAF tracks at 2- (C), 8- (D), and 12-second (E) event duration thresholds following SAHA (green data points and line) or DMSO (blue data points and line) treatment.

Figure 7: Model of bromodomain dependent effects on PBAF and PBAF binding within transcriptionally active euchromatic regions versus heterochromatic

regions. A. Increases in histone acetylation through SAHA treatment leads to an increase in the number of regions that experience re-visiting by the PBAF chromatin remodeling complex. Residence times also increase as shown through our territorial binding analysis. B. PBAF resides in H3.3-rich euchromatin for a shorter duration of time than within HP1α-rich heterochromatin.

Figure 1.

A Single molecule imaging of PBAF in live U2OS cells

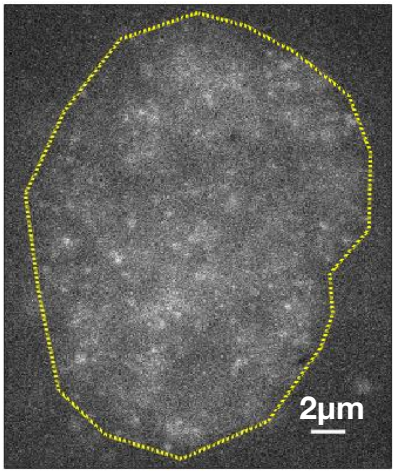

B Localization of PBAF binding events

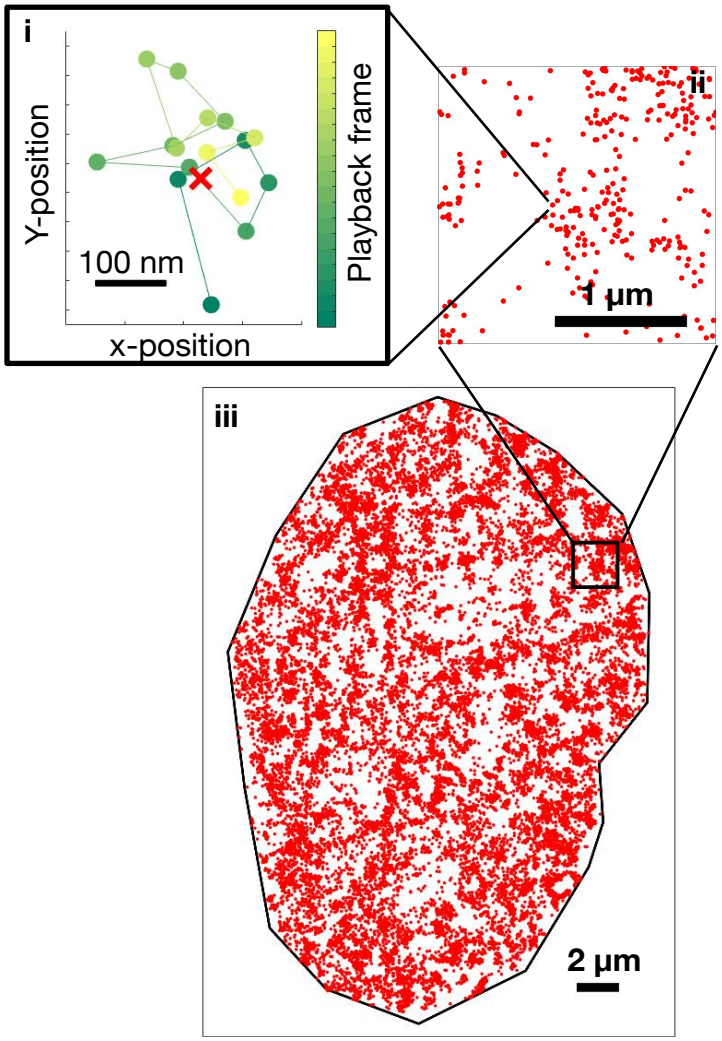

C Residence time of PBAF binding events

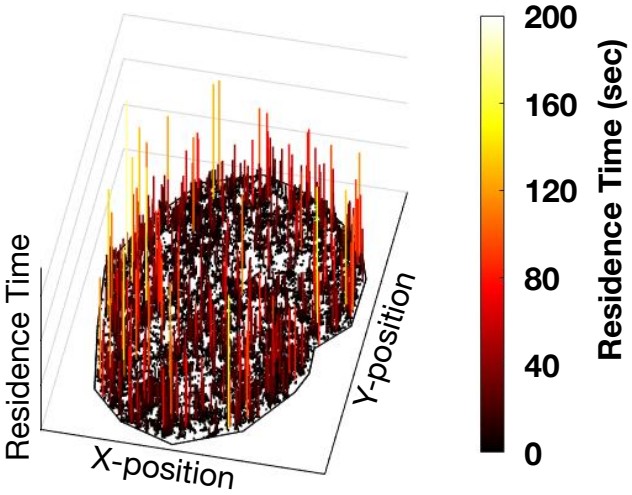

D Probability distribution of PBAF residence time

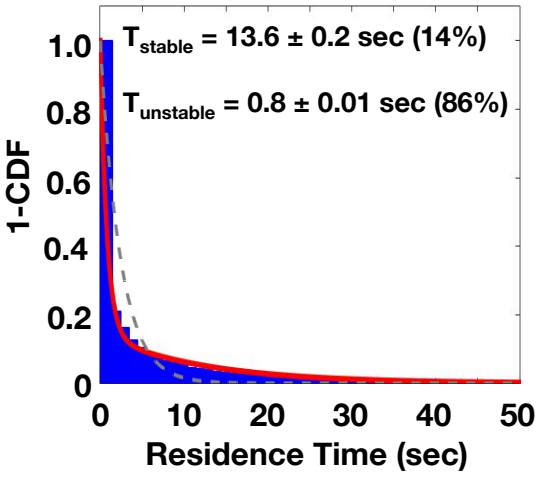

E

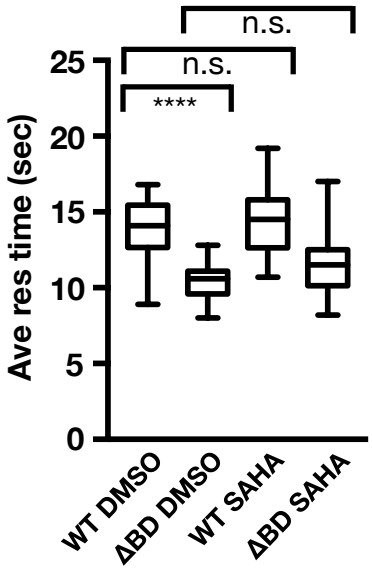

Figure 2

Kenworthy et al_Fig. 2

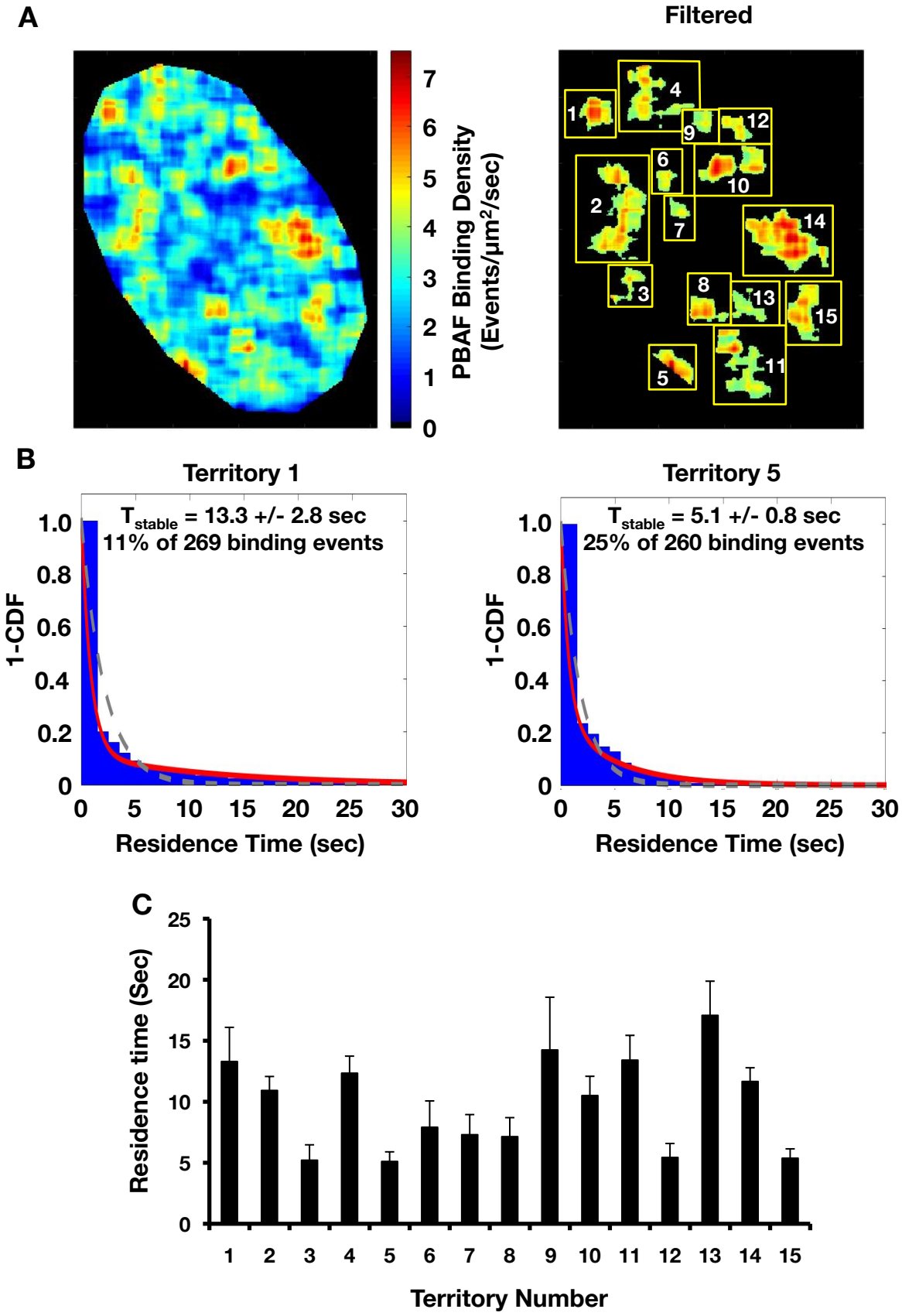

Figure 3

Kenworthy et al_Fig. 3

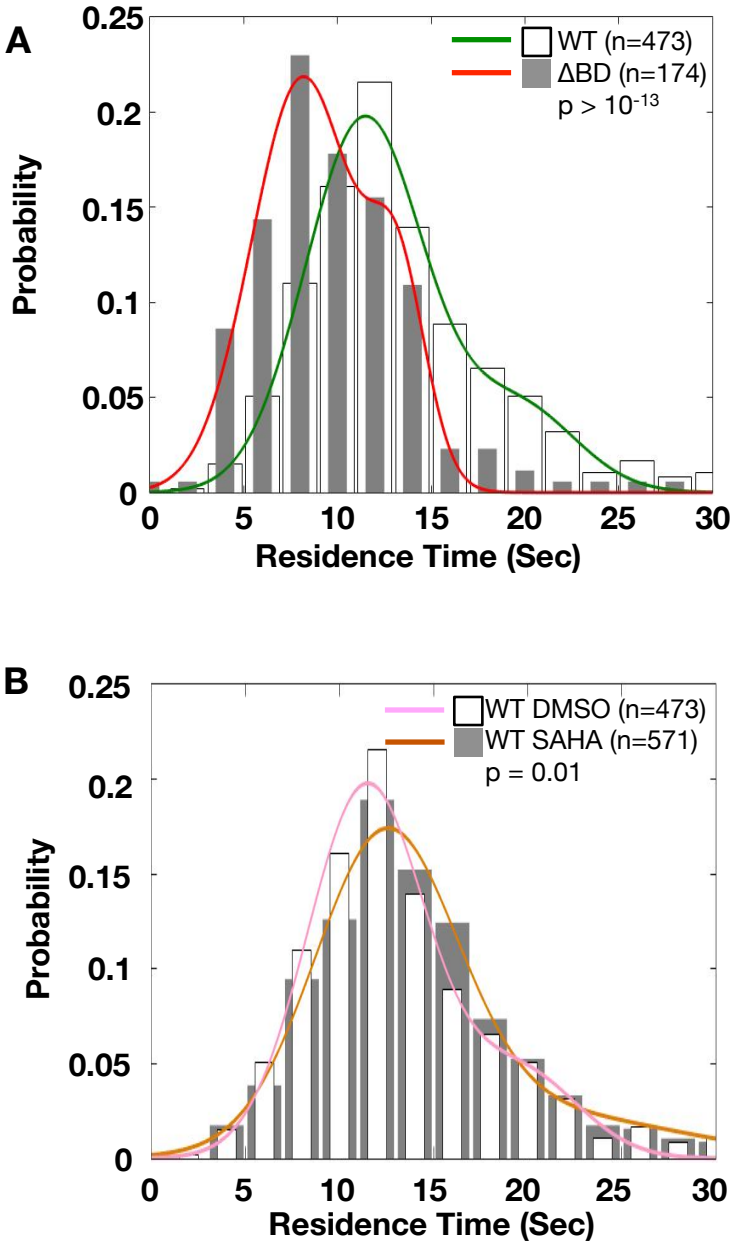

Figure 4

Kenworthy et al_Fig. 4

A

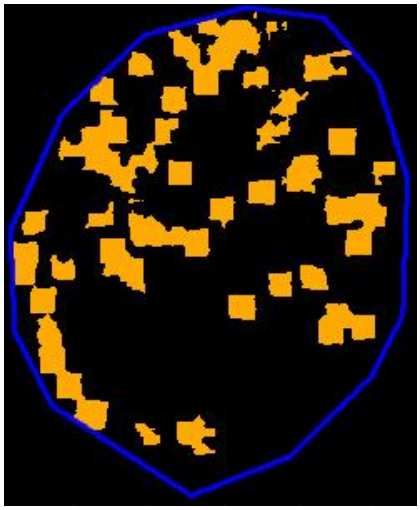

Density mapping of H3.3-SNAP

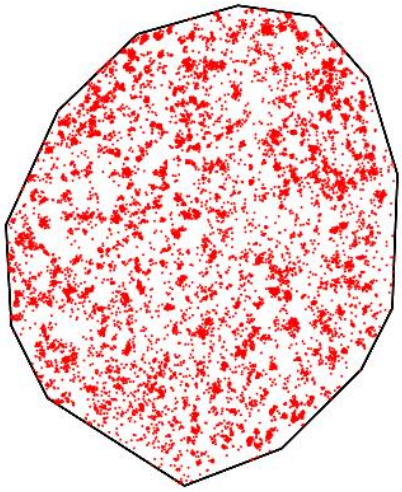

SPT mapping of Halo-BAF180WT

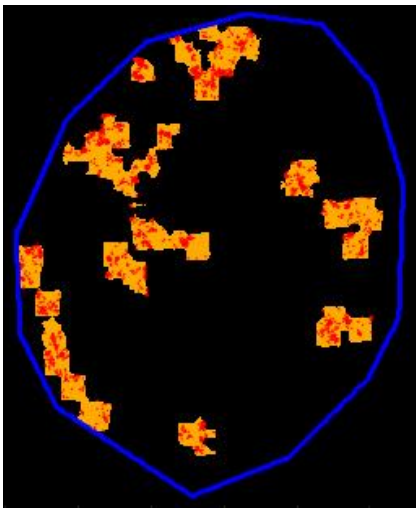

Masking of Halo-BAF180WT binding events within H3.3-SNAP territories, filtering, and SPT characterization.

B

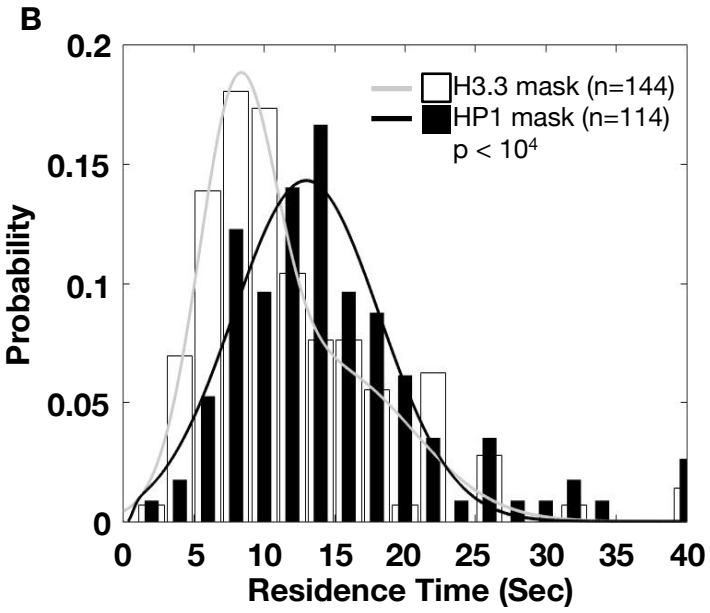

Figure 5

Kenworthy et al_Fig. 5

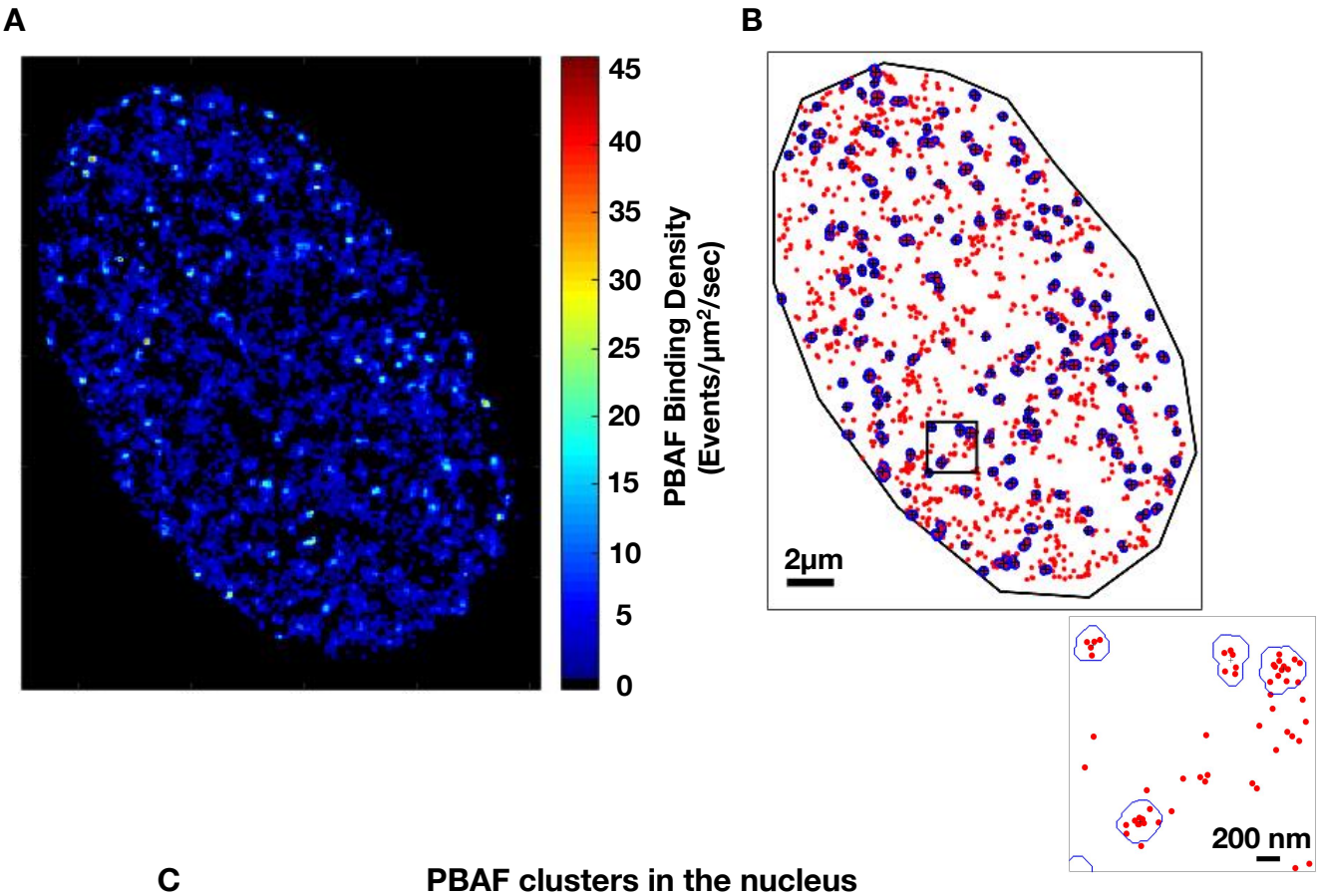

Figure 6

Kenworthy et al_Fig. 6

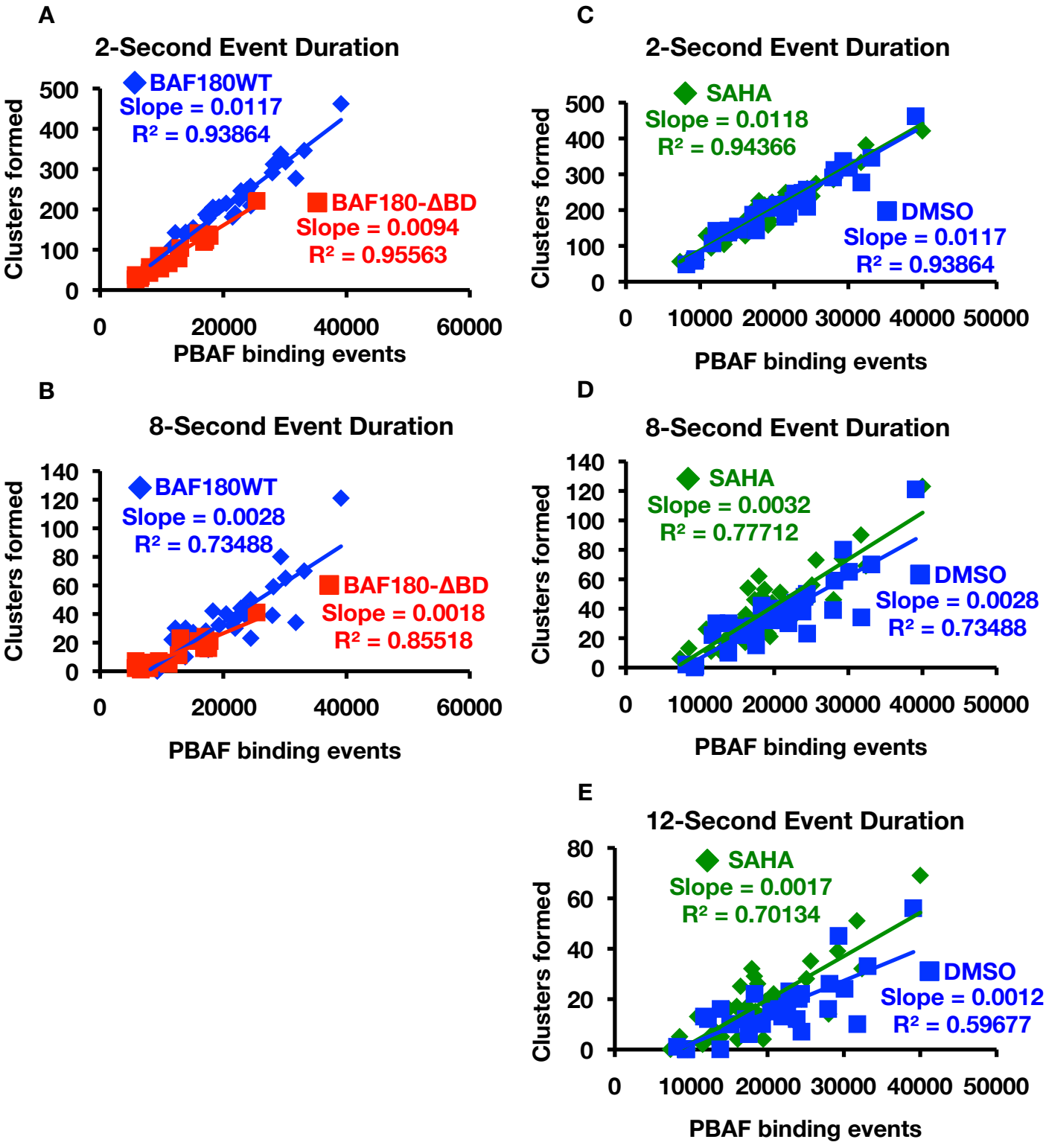

Figure 7

Kenworthy et al_Fig. 7